Electromagnetic Wave Chaos in Gradient Refractive Index Optical Cavities

P. B. Wilkinson,[1] T. M. Fromhold,[1] R. P. Taylor,[2] and A. P. Micolich[2]

[1]*School of Physics and Astronomy, University of Nottingham, Nottingham NG7 2RD, United Kingdom*

[2]*Physics Department, University of Oregon, Eugene, Oregon 97403-1274*

(Received 28 November 2000)

Electromagnetic wave chaos is investigated using two-dimensional optical cavities formed in a cylindrical gradient refractive index lens with reflective surfaces. When the planar ends of the lens are cut at an angle to its axis, the geometrical ray paths are chaotic. In this regime, the electromagnetic mode spectrum of the cavity is modulated by both real and ghost periodic ray paths, which also "scar" the electric field intensity distributions of many modes. When the cavity is coupled to waveguides, the eigenmodes generate complex series of resonant peaks in the electromagnetic transmission spectrum.

DOI: 10.1103/PhysRevLett.86.5466 PACS numbers: 42.65.Sf, 05.45.Mt, 42.25.Fx

The study of billiard systems, in which a particle is confined in a two-dimensional (2D) potential well, has led to key advances in our understanding of quantum chaos. For example, scarred wave functions, in which the probability density is concentrated along an unstable periodic classical orbit, were first identified in numerical studies of the stadium billiard [1]. They were subsequently observed in experiments on both 2D stadium-shaped microwave cavities [2] and semiconductor quantum dots [3]. Wave function scarring also has a pronounced effect on the current-voltage $I(V)$ characteristics of resonant tunneling diodes (RTDs) in a tilted magnetic field [4]. Together, the hard walls of the quantum well in the RTD and the soft parabolic magnetic potential form an unusual 2D billiard with chaotic electron dynamics. This type of billiard supports a hierarchy of unstable and stable periodic orbits. But the electron scattering rate due to LO phonon emission is so high that $I(V)$ measurements only resolve quantized states corresponding to short periodic orbits [4].

In this Letter, we show that light rays in a commercial gradient refractive index (GRIN) lens [5] with perfectly reflecting surfaces and tilted planar ends follow chaotic paths analogous to those of an electron in a RTD. The electromagnetic eigenmodes of the lens exhibit spectral fluctuations and scarring associated with many unstable periodic ray paths. We show that these effects should produce strong fluctuations in laser transmission experiments. In contrast to the RTD, the coherence length of laser light ($\gtrsim$1 m) greatly exceeds the dimensions of the GRIN lens. This permits the resolution, even at room temperature, of resonances associated with long complicated ray paths.

GRIN lenses are commercially available with a range of sizes and index profiles and their ends can be polished optically flat with any desired tilt angle. Here we consider a particular cylindrical lens [5] whose index profile is $n(y) = n_0(1 - \alpha^2 y^2)^{\frac{1}{2}}$, where $n_0 = 1.5$, $\alpha = 608.84\ \mathrm{m}^{-1}$, and y is the radial distance from its axis. Its length and diameter are $L = 2.58 \times 10^{-3}$ m and $W = 10^{-3}$ m, respectively. Ray paths within the lens are generally helical, like electron orbits in a magnetic field. But rays passing through the axis (meridional rays [6]) follow planar sinusoidal paths, which undergo specular reflection at the silvered surfaces. Each reflected ray follows a new sinusoidal path in the same plane as the incident ray. Consequently, the lens forms a 2D cavity for meridional rays. We have investigated how the ray dynamics depend on the tilt angle β of the planar ends (Fig. 1a). When $\beta = 0°$, the ray paths are regular and stable (Fig. 1b); but when $\beta \neq 0°$, the angled end surfaces interrupt the regular sinusoidal segments of the meridional rays at irregular times, thereby generating chaotic 2D ray dynamics (Fig. 1c) similar to those of electrons in the RTD [4]. The GRIN medium is essential for creating the chaotic ray paths, in contrast to previous studies of chaotic rays in deformed optical fibers with a constant refractive index [7]. Without the index variation, the parallelogram-shaped cavity would belong to the so-called "pseudointegrable" class of systems which have *nonchaotic* dynamics [8]. The smooth refractive index profile (analogous to the effective parabolic potential for an

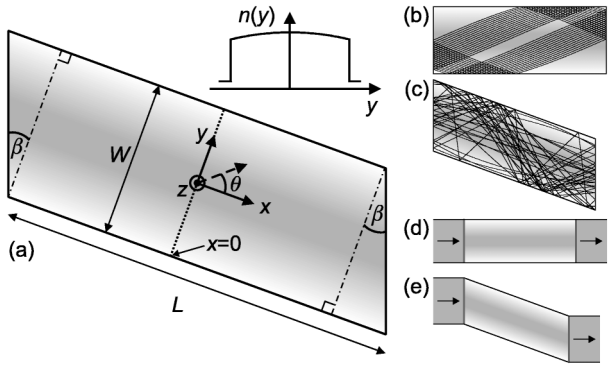

FIG. 1. (a) Schematic diagram of 2D closed cavity for meridional rays in a GRIN lens with reflective surfaces, showing tilt angle β of planar ends. The dashed line shows the direction of the ray path at $x = 0$ (dotted line) relative to the x and y axes. Gray-scale shading shows refractive index variation (gray: high; white: low). The upper inset shows refractive index profile $n(y)$. (b) A regular ray path ($\beta = 0°$). (c) A chaotic ray path ($\beta = 20°$). (d)(e) GRIN cavities with semisilvered ends attached to semi-infinite waveguides (solid dark gray) with constant refractive index and fully silvered walls. Arrows represent in- and outgoing modes.

 0031-9007/01/86(24)/5466(4)$15.00

electron in a magnetic field [4]) and impenetrable boundary walls make an interesting hybrid system with characteristics of both the RTD and traditional flat-bottomed 2D billiards.

To quantify the transition to chaotic dynamics, Fig. 2 shows Poincaré sections (slices through phase space) generated by plotting y and θ (see Fig. 1) each time the ray path intersects the line $x = 0$ with $dx/dt > 0$. At $\beta = 0°$, the points lie on concentric elliptical rings (Fig. 2a) showing that the ray paths are stable. When β is increased to 10° (Fig. 2b) the phase space reveals large KAM islands of stability [9] embedded in a chaotic sea. At $\beta = 20°$ (Fig. 2c) the phase space is almost completely chaotic and contains very few stable islands, which are too small to show up in the figure.

We consider how the onset of chaotic ray dynamics affects the electromagnetic modes of the planar cavity. For a given angular frequency ω these modes satisfy the wave equation

$$\nabla^2\mathbf{E} + k^2 n^2(y)\mathbf{E} = -\nabla\left(\mathbf{E}\cdot\frac{\nabla n^2(y)}{n^2(y)}\right), \qquad (1)$$

where $\mathbf{E}$ is the electric field, $n^2(y)$ is the spatially varying refractive index, and $k = \omega/c$ is the free space wave number. In general, the term on the right-hand side of Eq. (1) couples the spatial components of $\mathbf{E}$, causing the polarization of the wave to change with time. But we consider cavity modes in the (x, y) plane with $E_x = E_y = 0$ (TM modes). For these modes, the right-hand side of Eq. (1) is zero as $\mathbf{E}$ and ∇n^2 are orthogonal. The nonzero field component $E_z(x, y)$ *exactly* obeys a scalar wave equation

$$\frac{\partial^2 E_z}{\partial x^2} + \frac{\partial^2 E_z}{\partial y^2} + k^2 n^2(y) E_z = 0 \qquad (2)$$

analogous to the 2D Schrödinger equation. The boundary conditions for TM modes ($E_z = 0$) are identical to those for a particle in a quantum billiard. This analogy allows us to analyze this system using the theories of quantum chaos.

The density of the eigenmodes (which have discrete wave numbers $k = k_j$, $j = 1, 2, 3, \ldots$) can be written

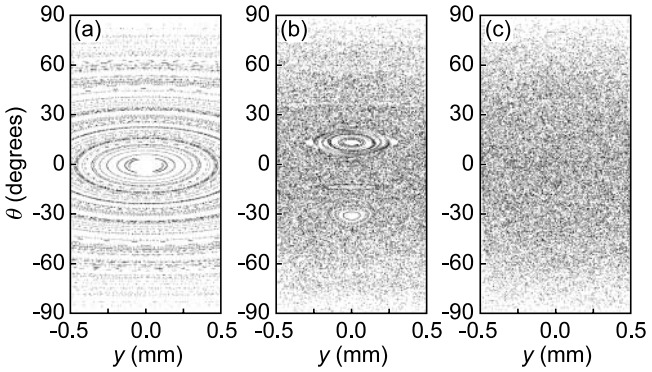

FIG. 2. Poincaré sections showing coordinates (y, θ) for rays crossing the plane $x = 0$ traveling from left to right in Fig. 1a. (a) $\beta = 0°$. (b) $\beta = 10°$. (c) $\beta = 20°$.

$$\rho(k) = \sum_j \delta(k - k_j) = \bar{\rho}(k) + \tilde{\rho}(k), \qquad (3)$$

where $\bar{\rho}(k)$ is a smooth, monotonically increasing average density and $\tilde{\rho}(k)$ is the remaining fluctuating contribution, analogous to that given by the semiclassical trace formula (TF) for a quantum chaotic system [9]. It follows from the TF that the contribution to $\tilde{\rho}(k)$ from a periodic ray of optical path length Λ is given by

$$F(\Lambda) \approx \int_0^{k_{\max}} \tilde{\rho}(k) U(k) \exp(-ik\Lambda)\, dk, \qquad (4)$$

where $k_{\max}$ is the wave number of the highest eigenmode considered and $U(k)$ is the Welch window function which suppresses ringing in the Fourier transform. We used a compact fourth-order finite-difference method [10] to calculate accurately the first 400 eigenmodes of the chaotic system with $\beta = 20°$. The power spectrum of $F(\Lambda)$ shown in Fig. 3 reveals a series of numbered peaks at Λ values equal to the optical path lengths of the associated periodic ray paths. Peaks 1 and 2 correspond, respectively, to single and double traversals of a simple "bouncing-ball" ray path across the cavity. There is a nonisolated family of these marginally stable paths which have previously been identified in chaotic stadium billiards [11]. Peaks 4–10, 12, and 14 are associated with progressively more complicated periodic ray paths involving multiple reflections from the cavity walls. There are also three additional peaks (3, 11, and 13) for which no periodic path exists. They correspond to "ghosts" [12] of the stable periodic

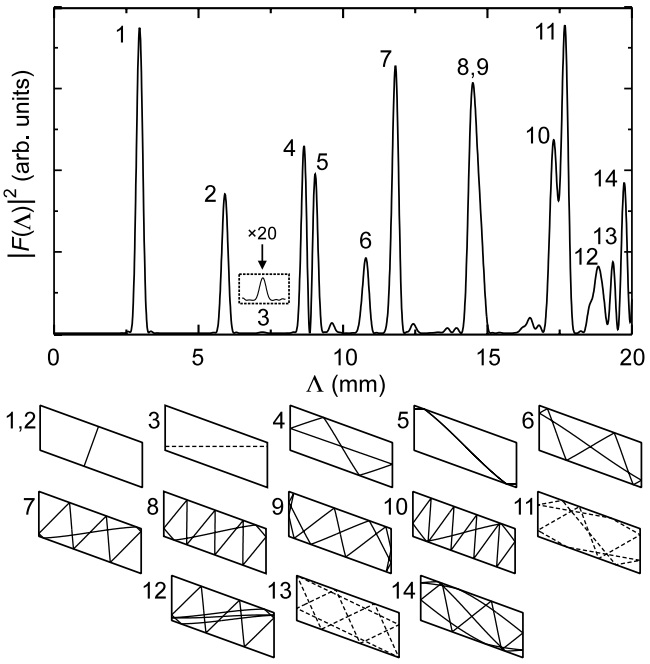

FIG. 3. Top: Fourier power spectrum of density of modes as a function of optical path length Λ, showing numbered peaks. The inset box shows peak 3 vertically magnified by factor of 20. Bottom: real (solid line) and ghost (dashed line) periodic ray paths which correspond to the peaks indicated by the numbers to the left of each path.

trajectories 3, 11, and 13 that are found in a cavity of the same shape but with a *constant* refractive index.

The GRIN cavity has great potential as an experimental probe of wave chaos. To illustrate this we calculate the transmission properties of two cavities with $\beta = 0°$ (Fig. 1d) and $\beta = 20°$ (Fig. 1e) which are weakly coupled to planar waveguides of width $W/\cos\beta$, with fully silvered walls [which are perpendicular to the (x, y) plane]. The waveguides are semi-infinite in extent in x and have a constant refractive index n_0. The weak coupling is achieved by semisilvering the ends of the cavity so that the reflection coefficient of each individual end surface is ~ 0.98 in the frequency range under consideration. To calculate the transmission coefficient, T, of the system, we solved Eq. (2) matching the solution across the semisilvered ends to linear combinations of both propagating and evanescent guided modes in the input (left) and output (right) waveguides. T, the ratio of the power in the incident and transmitted modes, is found by calculating their Poynting vectors. In our calculations, only a single incident propagating mode (the lowest) is used. We note that this is possible experimentally [13] and emphasize that similar results are obtained for other incident modes and lead refractive index profiles.

Figure 4a shows T versus ω for $\beta = 0°$ (stable ray paths). The graph exhibits sharp peaks at ω values for which a half-integer number of wavelengths fits along the cavity. These are Fabry-Perot resonances with a period of $\Delta\omega = 2\pi c/n_0 L = 2.44 \times 10^{11}$ rad s^{-1}. In addition, five much smaller peaks (arrowed) are present. These are due to the incident mode (with one lateral antinode across the y direction) coupling weakly to Fabry-Perot-like states in the cavity with three lateral antinodes. This coupling occurs because the modes in the waveguides and the resonant states in the cavity have slightly different y dependencies, arising from the different refractive index profiles. The vertical lines in Fig. 4a show the angular frequencies of the eigenmodes of the closed cavity shown in Fig. 1b. The solid lines indicate the small subset of modes which correspond to the resonant peaks in $T(\omega)$. Since E_z vanishes at the ends of the closed cavity for these modes, their angular frequencies are slightly higher than the ω values corresponding to resonant transmission through a cavity with semisilvered ends.

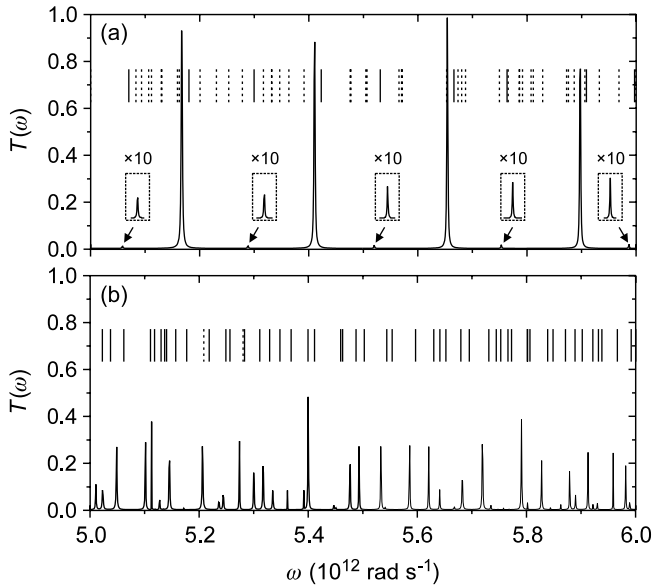

FIG. 4. (a) Transmission spectrum of the weakly coupled cavity with $\beta = 0°$ (Fig. 1d) showing strong and weak (arrowed, vertically magnified by 10) transmission peaks. Vertical lines indicate the angular frequencies of the eigenmodes of the corresponding closed cavity. Solid lines mark eigenmodes related to the resonant peaks. (b) As (a) with $\beta = 20°$.

Figure 4b shows the $T(\omega)$ plot and closed cavity eigenfrequencies (vertical lines) corresponding to the strongly chaotic ray dynamics at $\beta = 20°$. At each peak in $T(\omega)$, the distribution of electric field intensity in the cavity closely matches that of a closed cavity eigenmode. Unlike Fig. 4a, all but two of the eigenmodes produce discernible peaks. This means that even though only one mode is excited in the incident wave, almost the entire eigenmode spectrum of the associated closed system can be probed by measuring $T(\omega)$. By contrast, in RTDs only a small number of eigenstates are accessible to experiment due to tunneling selection rules [4].

In quantum chaotic systems, unstable periodic orbits scar subsets of wave functions [1–4]. An analogous effect, a concentration of electric field intensity along an unstable periodic ray path, occurs in many of the resonant modes of the weakly coupled GRIN cavity. Figure 5 shows the electric field intensity distributions at five different frequencies. Each of these distributions is scarred by the unstable periodic ray path shown overlaid. Of particular note is mode (b), which is concentrated along the ghost path associated with peak 3 in Fig. 3. Also shown in Fig. 5 are the Wigner functions of each scarred mode

$$\gamma(y, \theta) \propto \int E_z(\mathbf{r} + \mathbf{l}) E_z(\mathbf{r} - \mathbf{l}) \exp[-2ikn(\mathbf{r})\mathbf{s} \cdot \mathbf{l}]\, d\mathbf{l}, \tag{5}$$

which give a phase space representation of the electric field distribution analogous to the classical Poincaré section [14]. In Eq. (5), $\mathbf{r} = (x, y)$, $\mathbf{l}$ is a displacement from $\mathbf{r}$ in the (x, y) plane, and $\mathbf{s} = (\cos\theta, \sin\theta)$. The Wigner functions are calculated for $x = 0$, as are the Poincaré sections in Fig. 2. The large positive values of γ (white) are centered on the initial coordinates (y, θ) of the corresponding scarring ray paths. This provides clear evidence that the scar patterns originate from these ray paths.

The density of modes modulation and eigenmode scarring should both be experimentally observable. We propose to excite resonant modes within the cavity with a tunable laser source, measuring the transmitted power directly with photodetectors. GRIN lenses and optical fiber components are usually optimized to work at optical or near infrared (NIR) wavelengths. At the widely used NIR wavelength $\lambda = 1550$ nm, the average frequency spacing

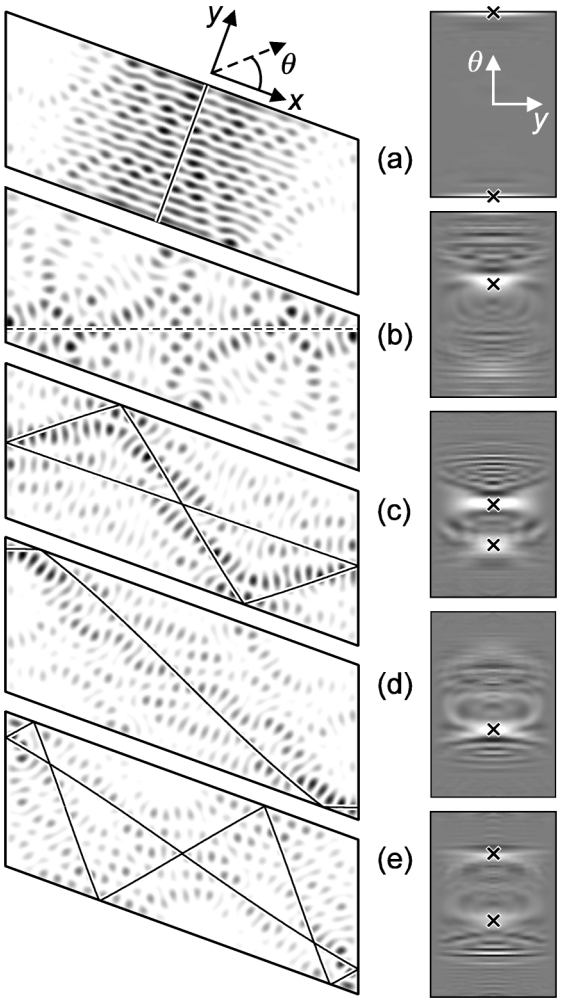

FIG. 5. Left: Electric field intensity (white = 0) in the x-y plane [axes shown above (a)] for weakly coupled cavity modes with $\beta = 20°$. Scarring real (ghost) paths are shown by solid (dashed) overlays. Right: Corresponding Wigner functions $\gamma(y, \theta)$ (black $\ll 0$, gray $= 0$, and white $\gg 0$) with coordinate axes overlaid on (a). The coordinate ranges are -0.5 mm $< y < 0.5$ mm and $0° < \theta < 90°$, as in Fig. 2. Crosses indicate initial coordinates of the scarring ray paths. The angular frequencies are (a) 8.941×10^{12} rad s^{-1}, (b) 7.913×10^{12} rad s^{-1}, (c) 8.726×10^{12} rad s^{-1}, (d) 8.855×10^{12} rad s^{-1}, (e) 8.803×10^{12} rad s^{-1}.

between adjacent eigenmodes in the GRIN cavity is $\sim$13 MHz. To resolve peaks in $T(\omega)$ corresponding to individual eigenmodes would therefore require a laser with linewidth and tuning precision of $\sim$1 MHz. Linewidths of this order have been reported in tunable lasers [15]. Alternatively, we could measure T as a function of temperature at fixed ω. Thermal expansion would change the size of the cavity and thereby alter the optical path lengths of the periodic rays, with transmission maxima occurring for quantized values of Λ/λ. For typical coefficients of thermal expansion and thermal refractive index variation [16], the average temperature spacing between adjacent resonances would be between 0.01 and 0.1 K. This method has analogies with studies of chaotic semiconductor billiards in which the transport properties of a two-dimensional electron gas with a fixed Fermi energy are probed as a function of magnetic field [3]. Working at a fixed frequency might also allow direct observation of the eigenmodes of GRIN cavities doped with erbium ions. At 1550 nm, Er ions luminesce and the patterns of luminescence intensity, observed through unsilvered windows in the upper and lower ($z \neq 0$) surfaces of the sample, would directly reveal the spatial distribution of the cavity eigenmode with subwavelength resolution [17].

In summary, we have shown that meridional rays in a commercially available GRIN lens with tilted planar ends exhibit chaotic dynamics analogous to electron motion in both RTDs and sub-micron-sized electron billiards. In contrast to these semiconductor systems, high resolution measurements of the mode spectrum of the GRIN lens should be possible even at room temperature. Such experiments could provide insights for understanding the quantum properties of analogous electronic systems with mixed stable/chaotic dynamics, which are of topical interest and beyond the scope of current theories [18]. They could also investigate the effects of chaotic nonmeridional ray paths on the three-dimensional electromagnetic modes of the cylindrical lens (which are solutions of the full vector wave equations). Since GRIN materials are well developed and widely used in optoelectronics and telecommunications, they might provide a natural route to the technological exploitation of ray and wave chaos.

This work is supported by EPSRC UK. We are grateful to Dr. S. A. Brown for helpful discussions about Er doping.

[1] E. J. Heller, Phys. Rev. Lett. **53**, 1515 (1984).
[2] S. Sridhar and E. J. Heller, Phys. Rev. A **46**, R1728 (1992); H.-J. Stöckmann, *Quantum Chaos: An Introduction* (Cambridge University Press, Cambridge, 1999).
[3] C. M. Marcus *et al.,* Phys. Rev. Lett. **69**, 506 (1992); J. P. Bird *et al.,* Phys. Rev. Lett. **82**, 4691 (1999).
[4] P. B. Wilkinson *et al.,* Nature (London) **380**, 608 (1996).
[5] Lenses made from SELFOC glass, Nippon Sheet Glass Company Ltd., Type of lens: SLW 1.0 0.25 0.63 NC.
[6] J. A. Buck, *Fundamentals of Optical Fibers* (Wiley, New York, 1995).
[7] J. U. Nöckel and A. D. Stone, Nature (London) **385**, 45 (1997); C. Gmachl *et al.,* Science **280**, 1556 (1998).
[8] A. Shudo *et al.,* Phys. Rev. E **49**, 3748 (1994).
[9] E. Ott, *Chaos in Dynamical Systems* (Cambridge University Press, Cambridge, 1993).
[10] P. B. Wilkinson *et al.,* Physica (Amsterdam) **272B**, 484 (1999).
[11] H. Alt *et al.,* Phys. Rev. E **60**, 2851 (1999).
[12] P. Bellomo and T. Uzer, Phys. Rev. A **51**, 1669 (1995).
[13] F. Dubois *et al.,* Opt. Lett. **19**, 433 (1994).
[14] P. A. Dando and T. S. Monteiro, J. Phys. B **27**, 2681 (1994).
[15] T. Kiguchi *et al.,* Jpn. J. Appl. Phys. **35**, 5890 (1996).
[16] P. O. McLaughlin and D. T. Moore, Appl. Opt. **24**, 4334 (1985).
[17] E. Snoeks *et al.,* J. Opt. Soc. Am. B **12**, 1468 (1995).
[18] J. Main and G. Wunner, Phys. Rev. Lett. **82**, 3038 (1999).